Sub-millisecond microfluidic mixers coupled to time-resolved in-situ photonics to study ultra-fast reaction kinetics. The case of ultra-small gold nanoparticles synthesis.

Raj Kumar Ramamoorthy,[1,2,3] Ezgi Yildirim,[1] Isaac Rodriguez-Ruiz,[2,*] Pierre Roblin,[2] Lise-Marie Lacroix,[1,5] Ana Diaz,[4] Rohan Parmar,[2] Sébastien Teychené, [2] Guillaume Viau [1,*]

[1] Université de Toulouse, Laboratoire de Physique et Chimie des Nano-Objets UMR 5215 INSA, CNRS, UPS, 135 avenue de Rangueil F-31077 Toulouse cedex 4, France

[2] Laboratoire de Génie Chimique, Université de Toulouse, CNRS, INP, UPS Toulouse, France

[3] Fédération de Recherche, Université de Toulouse, CNRS, INP, INSA, UPS, Toulouse France

[4] Paul Scherrer Institute, Villigen PSI, Switzerland

[5] Institut Universitaire de France (IUF), 103 boulevard Saint Michel, 75005 Paris, France

Supporting information document

The reactors (Figure S1) were fabricated by injection moulding on a PDMS mold fabricated by standard soft lithography techniques. Briefly, OSTEMER material, which is based on thiol–ene click chemistry (Hoyle & Bowman, 2010), is an off-stoichiometry thiol–alkene–epoxy polymer with two different curing steps. In the first step, the OSTEMER liquid formulation is injected through a PDMS mold (see injection process scheme in figure S2). In the case of UV-Vis microreactors, the mold is placed against a disposable mylar film, whereas in the case of XAS and SAXS reactors a Kapton film is used against the PDMS mold for OSTEMER direct injection. The mold and the film are placed between 2 glass slides and clamped in order to avoid leaks during OSTEMER injection (Figure S2 I, and S2 a, S2 b)The liquid formulation is subsequently injected manually with the help of a needle and a syringe (Figure S2 II). For this step, several cylindrical pillar-like structures have been conceived across the whole microreactors structures (see figure S1), serving to ease OSTEMER spreading during injection, and at the same time defining a constant and uniform reactor thickness. After the PDMS mold is filled with the liquid OSTEMER formulation, a first reticulation step by UV curing takes place. The PDMS mold, imprinting the shape and determining the thickness of the mixer and channel structures can be removed after this first reticulation. At this step, the UV-cured OSTEMER becomes solid because of the thiol-alkene crosslinking, but flexible and yet sticky due to the remaining free epoxy groups. The main role of the disposable mylar here is to serve as a carrier of the sticky OSTEMER structure, easing its manipulation (Figure S2 V, OSTEMER sticker figure S2c), while a Kapton film would serve both for manipulation and as a chip transparent X-ray window. As soon as the PDMS mold and the structure are separated, OSTEMER open channels can be auto-glued to a glass slide (in the case of the UV-Vis microreactor) or a second Kapton film (in the case of XAS and SAXS) microreactors to seal the structure, and epoxy cross-linking can be finished with a thermal curing stepA second OSTEMER layer, comprising the interface with microfluidic tubings and channels is subsequently added, and a final temperature-curing step completes the fabrication of the microreactors. In the case of X-Ray transparent platforms, hybrid OSTEMER–Kapton microchips were specifically fabricated using 75 µm thick Kapton windows (DuPont, France) to minimize X-ray background noise. Channels in this case are conceived as open structures by both sides, so the only material through the X-ray optical path is Kapton.

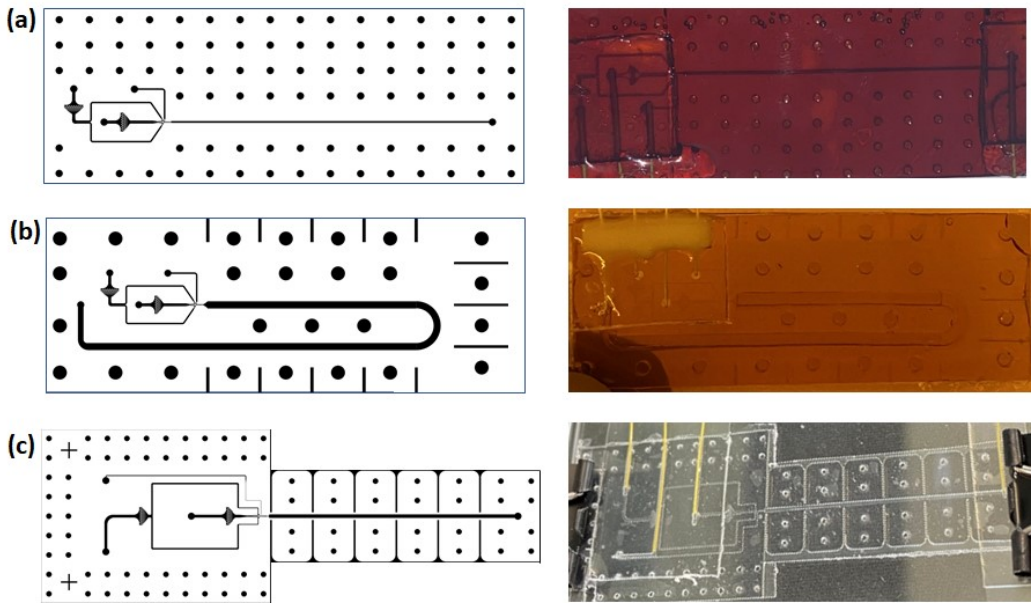

Figure S1. Schemes and picture of the 3 microreactors fabricated and used in this work. A) SAXS microreactor; b) XAS microreactor; c) UV-Vis microreactor

Microreactors fabrication by injection molding

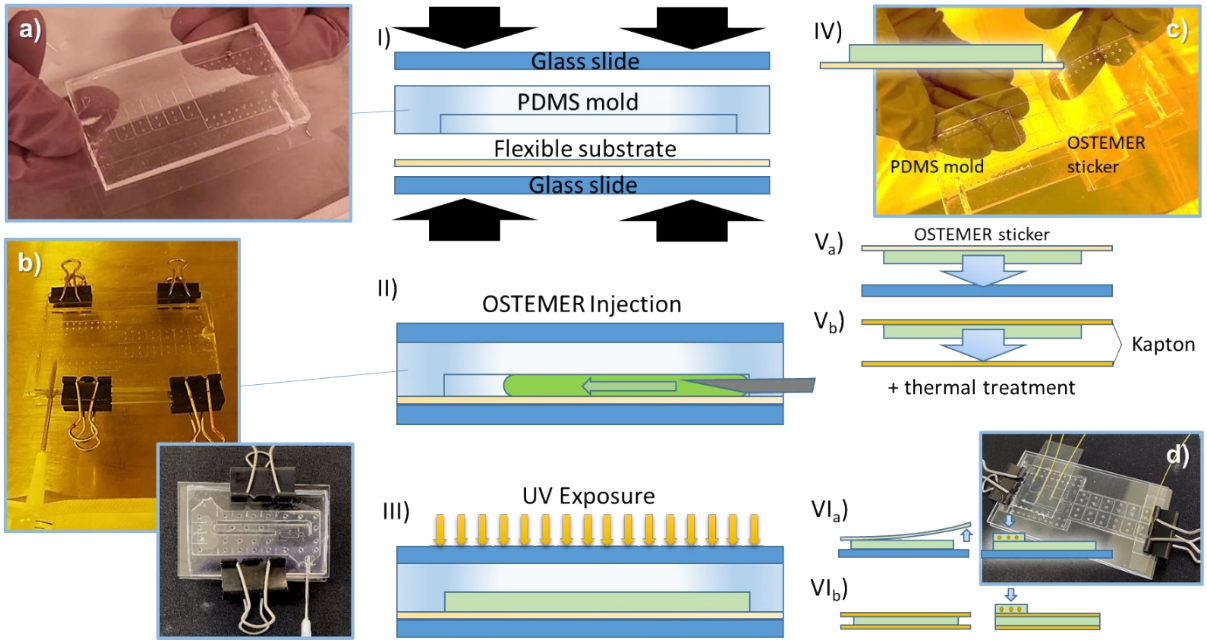

Figure S2. (I) PDMS mold (a) is placed between two glass slides with a flexible substrate (disposable Mylar or Kapton window) on one side and the ensemble is clamped for injection. (II) OSTEMER injection with the help of a needle through the PDMS mold (b). (III) UV exposure to cure the OSTEMER polymer. (IV) OSTEMER sticker holding the reactor structure on the flexible substrate/Kapton (c). (V) Transfer of the OSTEMER structure onto a glass slide (Va) or a second Kapton film (Vb) to close the fluidic structures. (VI) a second OSTEMER sticker is placed on top to allow a second fluidic level for a chip-to-world connection by means of 360 µm PEEK tubing (d).

XAS microreactors mold fabrication

The large optical path required to perform in-situ XAS analyses (1.9 mm) exceeds by far the usual microfluidic dimensions that can be attained by classical soft lithography. Hence a 2-step mold fabrication methodology has been developed, by combining resin 3D printing for the millifluidic structures and photoresist dry film lamination for the microfluidic structures. The main and larger millifluidic reactor features for the mold (figure S3a) were printed in commercial ABS-like resin using a low-cost Mars 2 3D printer (Elegoo, China). The reactor geometry consists on a 70 (30 + 40) mm channel with 2 Kapton windows, and comprising a 180 ° channel turn for the sake of compactness. In order to permit OSTEMER injection without trapping air bubbles in this turn, the thickness of the channel has been reduced locally to allow the circulation of liquid OSTEMER during injection through it (otherwise it would only circulate besides it to ensure fully open OSTEMER structures). This way and any possible air trapped between the two channel parts can be removed. Besides the main channel features, the 3D printed structure also comprises several side channels which have been included along the microdevice for X-ray beam alignment purposes. These channels serve to insert metal wires at well-defined places which can be easily spotted during a blind (no optical imaging required) X-ray microreactor scan, to immediately retrieve reactor coordinates and subsequently automatize data adquisition. The printed 3D structure (figure S3a) was glued on top of a glass slide and a dry film photoresist 50 µm layer (WBR 2050 Dupont, France) was subsequently laminated on top. The photoresist was exposed through an emulsion film photolithography mask and developed with a 1% w/w K_2CO_3 solution, revealing the microfluidic mixer structures imprinted by the mask (Figure S3b). Finally, the whole structure was treated with an anti-adherent coating (NOVEC 1710, 3M, US) to facilitate PDMS cast molding on it to retrieve the injection mold (detail of the mold in Figure S3c). The manual injection process implies a progressive damaging of the PDMS mold due to injection needle perforation. Hence, if the number of microreactors to be fabricated is large, several molds might be needed. To this end, it is possible to replicate the initial hybrid mold (of complex fabrication) by simply counter-molding the PDMS structure by OSTEMER injection against a glass slide, and use this OSTEMER structure (figure S3d) for subsequent replications.

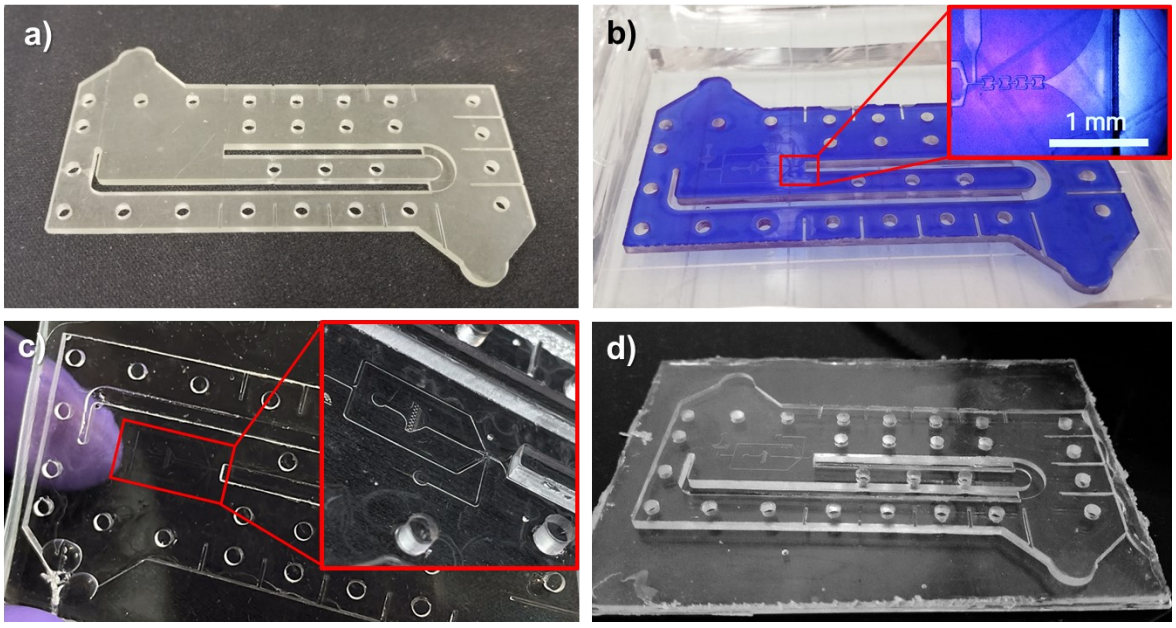

Figure S3. a) 3D printed structure including the main channel and alignment channel features. b)Hybrid mold comprising both 3D printed millifluidic and soft-lithography microfluidic structures laminated and developed on top. Inset shows a detail of the microfluidic butterfly mixer and the microfluidic-millifluidic interface. c) PDMS injection mold for XAS microreactor. Inset shows a detail on the microfluidic channels and beginning of the millifluidic reactor. d) OSTEMER replica of the hybrid microfluidic-millifluidic mold.

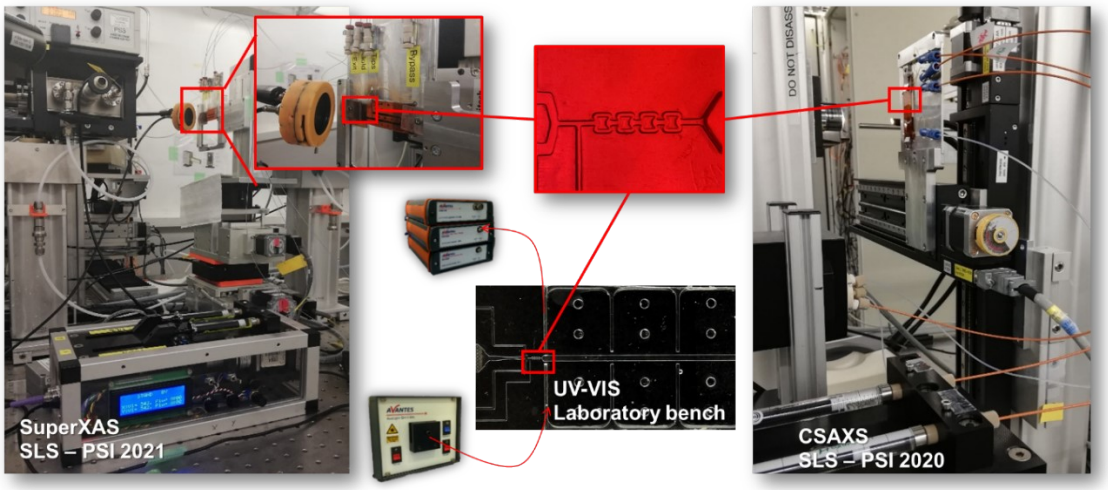

Figure S4. Pictures and schematics of the different microreactor setups installed in the synchrotron facilities and laboratory bench.

Method	[Reducing agent]	Population A		Population B		Relative proportion	
		d_m (nm)	σ/d_m (%)	d_m (nm)	σ/d_m (%)	% A	% B
batch	**[TIPS] = 62 mM**	1.8	17	3.5	15	65	35
	TIPS] = 125 mM	1.6	19	2.9	21	75	25
	[TIPS] = 250 mM	1.6	17	2.6	23	83	17
	[TIPS] = 1 M	1.7	15	2.6	23	87	13
microfluidic set-up	**[TIPS] = 62 mM**	1.8	9	2.6	24	77	23
	[TIPS] = 1 M	1.7	16	2	48	91.5	8.5

Table S1. Characteristics of the two populations observed in Au nanoparticles prepared with of different reducing agent concentration and following two protocols: synthesis in batch or using the microfluidic reactor. The reported parameters were deduced from the fit of the experimental SAXS patterns using two gaussian distributions (A and B). Population A refers to the ultrasmall NPs, population B to the larger NPs. d_m : mean diameter; the polydispersity expressed as σ/d_m, (with σ the standard deviation of the gaussian distribution).

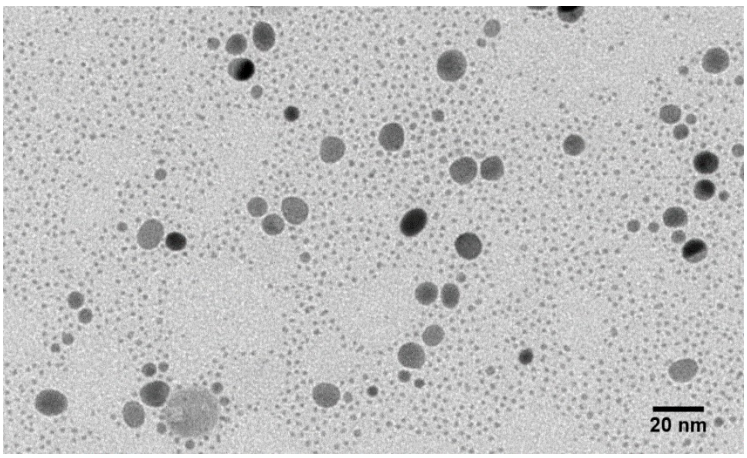

Figure S5. TEM image of the Au NPs obtained after 3h of reaction in presence of [TIPS] = 62 mM.

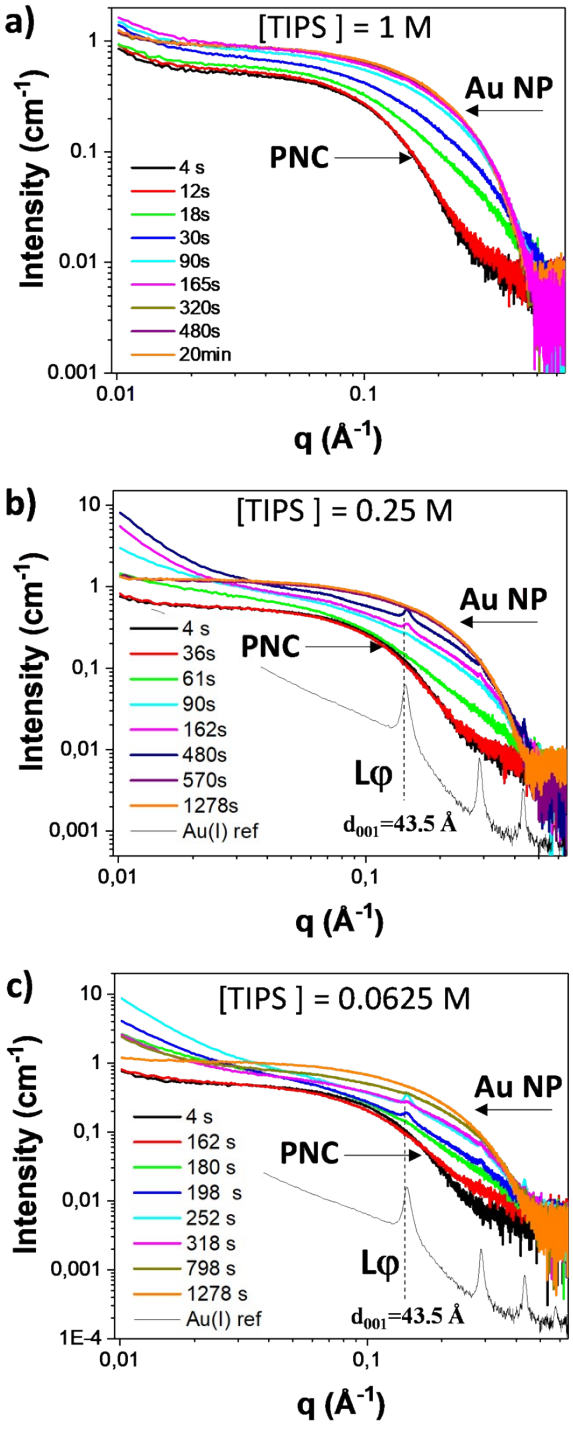

Figure S6. In situ SAXS pattern of the Au NPs formation with [TIPS] (a) 62 mM, (b) 250 mM and c) 1 M. First patterns at 4 s on (a), (b), and (c) correspond to the scattering signal of Au pre-nucleation clusters. Figure adapted from reference 44.

In the three graphs, the signal at short times corresponds to the pre-nucleation clusters of Au(III) and then of Au(III)-Au(I). This signal is referred to as PNC on the graphs. At a given time a shift of the "knee position" to high-q values is observed which correspond to the formation of small Au NPs in the medium. Then, the SAXS signal shift again to low q in a smaller extent and the intensity at low q is increasing significantly. This third stage is interpreted by the growth of the Au nanoparticles. The final SAXS signal is referred to as Au NP on the graphs. For the TIPS concentration of 62 mM and 125 mM the Bragg peaks of a lamellar phase are observed concomitantly to the nucleation stage. In black as an inset is given the SAXS pattern of the lamellar phase of formula Au(I)-Cl-oleylamine showing the same reticular distances (Lφ in the graphs). AT the end of the reaction the lamellar phase has disappeared. All the intermediate Au(I) species has been reduced in Au(0).

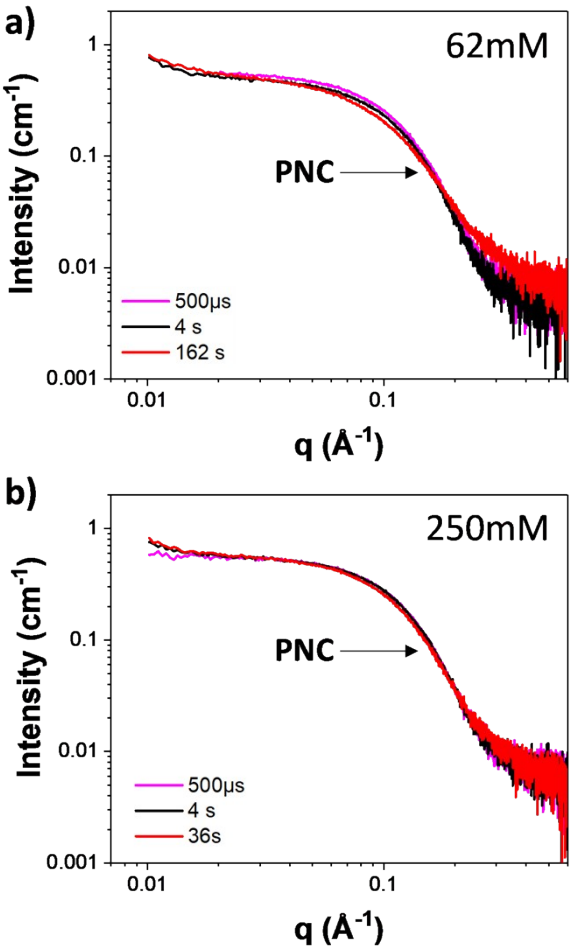

Figure S7. Time evolution of the in situ SAXS patterns recorded during the induction period observed in presence of [TIPS] a) 62 mM and b) 250 mM.

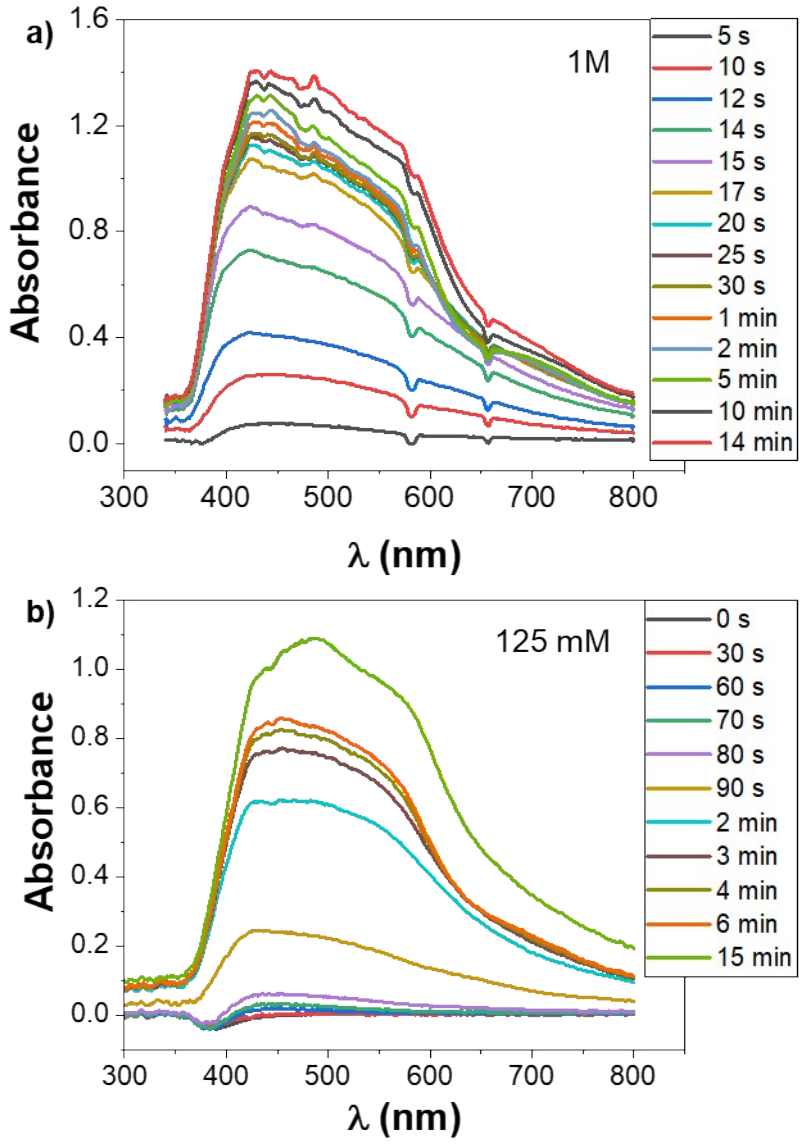

Figure S8. Time evolution of the *in situ* visible absorption spectra recorded during the Au NPs synthesis with a) [TIPS] = 1 M, b) [TIPS] = 125 mM

Kinetic models of the induction stage

Two chemical reactions were considered to describe the reduction of Au(III) to Au(I) during the induction stage, the direct reduction by the TIPS (Eq. S1) and an autocatalytic reaction (Eq. S2).

$$Au(III) + TIPS \xrightarrow{k_1} Au(I) \qquad \text{(Eq. S1)}$$

$$Au(III) + Au(I) \xrightarrow{k_{ac}} 2Au(I) \qquad \text{(Eq. S2)}$$

In the case of a direct reduction, the [Au(III)] reduction rate is written as:

$$-\frac{d[Au(III)]}{dt} = k_1[Au(III)] \times [TIPS] \quad \text{(Eq. S3)}$$

In large excess of TIPS, Eq. S3 can be simplified as:

$$-\frac{d[Au(III)]}{dt} = k_1'[Au(III)] \quad \text{(Eq. S4)}$$

The resolution of this first order reaction leads to an exponential decreases of [Au(III)] described by Eq. S5.

$$[Au(III)] = [Au(III)]_\infty + \left([Au(III)]_0 - [Au(III)]_\infty\right) \exp\left(-k_1' t\right) \quad \text{(Eq. S5)}$$

In the case of the autocatalytic reaction of Eq. 2, the [Au(III)] reduction rate is written as:

$$-\frac{d[Au(III)]}{dt} = k_{ac}[Au(III)] \times [Au(I)] \quad \text{(Eq. S6)}$$

When both reduction pathways occur, the [Au(III)] reduction rate is the sum of two terms:

$$-\frac{d[Au(III)]}{dt} = k_{ac}[Au(III)] \times [Au(I)] + k_1'[Au(III)] \quad \text{(Eq. S7)}$$

Taking into account that during the induction stage, i.e. before the Au(0) onset, $[Au(III)] + [Au(I)] = c_0$ (with c_0 the total concentration of gold), the resolution of Eq. S7 gives:

$$[Au(III)] = \frac{[Au(III)]_0 \times \left(k_{ac}c_0 + k_1'\right)}{\left(k_{ac}[Au(III)]_0 + \left(k_{ac}c_0 + k_1' - k_{ac}[Au(III)]_0\right)\exp\left[\left(k_{ac}c_0 + k_1'\right)t\right]\right)} \quad \text{(Eq. S8)}$$

In our case, the Au speciation curves were normalized taking $c_0 = 1$.

In the Figure S9 are given the relative Au(III) concentration versus time for the different TIPS concentration focusing on the induction stage. The [Au(III)] curves are concave for the TIPS concentrations of 62 mM, 125 mM and 250 mM indicating that an autocatalytic reaction is occurring in this time range. The [Au(III)] curves were nicely fitted with Eq. S8 for these TIPS concentrations (Fig. S8(a-c)). The ratio between the reaction constants k'_1/k_a, is equal to 0.05 for [TIPS] = 62 and 125 mM and it increases to 0.15 for [TIPS] = 250 mM, showing that the relative weight of the direct reduction increases significantly at higher TIPS concentration. For [TIPS] = 1 M, the [Au(III)] curve is no more concave and fits perfectly with a decreasing exponential described by Eq. S5 (Figure S9d), showing that the autocatalytic pathway is negligible compared to the direct reduction.

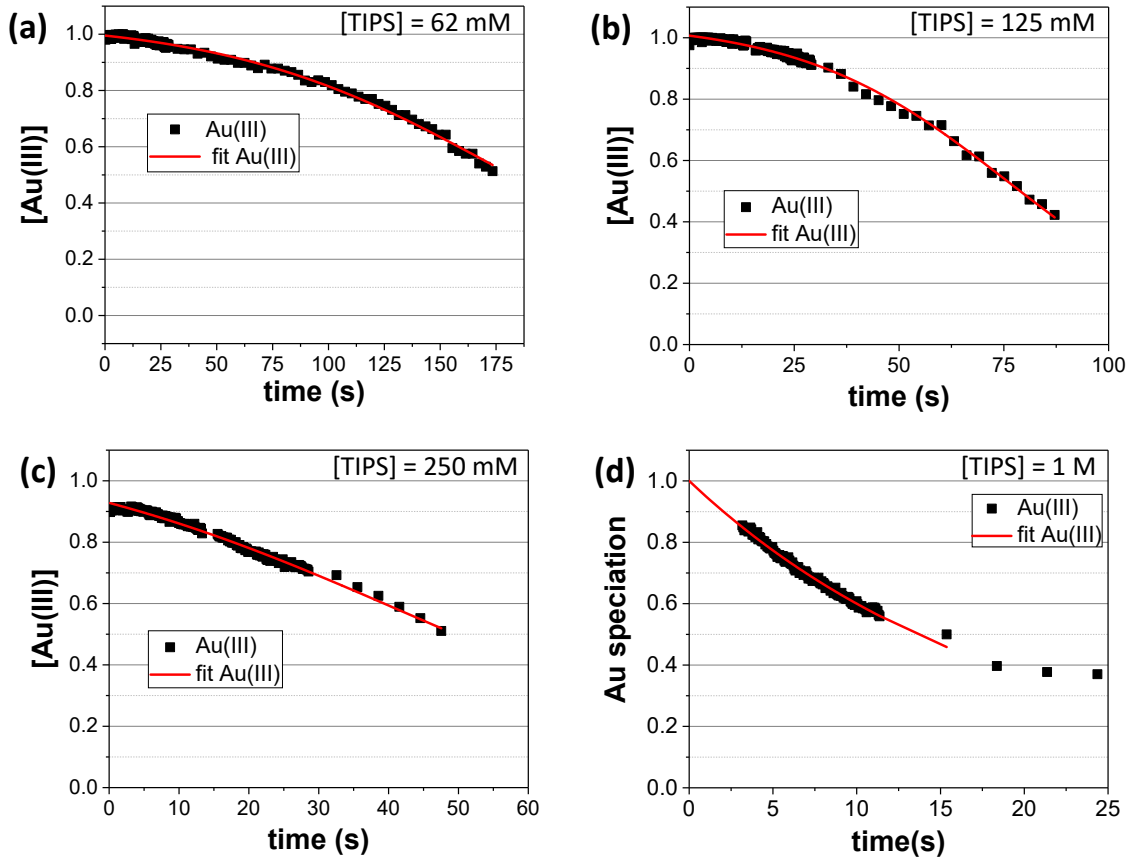

Figure S9. (a-c) Fit with Eq. S8 of the [Au(III)] curves during the induction period of the reactions carried out with (a) [TIPS] = 62 mM; (b) [TIPS] = 125 mM and (c) [TIPS] = 250 mM. The three parameters of the best fits were: (a) $[Au(III)]_o = 0.995$; $k_{ac} = 1.55\ 10^{-2}$; $k'_1 = 8.04\ 10^{-4}$; (b) $[Au(III)]_o = 1.00$; $k_{ac} = 3.82\ 10^{-2}$; $k'_1 = 2.04\ 10^{-3}$; (c) $[Au(III)]_o = 0.928$; $k_{ac} = 3.0\ 10^{-2}$; $k'_1 = 4.4\ 10^{-3}$. (d) Fit with Eq. S5 of the [Au(III)] curve during the induction period of the reaction carried out with [TIPS]= 1 M. The parameters of the best fit were: $[Au(III)]_\infty = 0.03$ and $k'_1 = 5.34\ 10^{-2}$.